

## **REDUCED PRECIPITATION ON RAPA NUI DURING THE DECLINE OF THE MOAI CULTURE**

Redmond Stein\*<sup>1</sup>, Lorelei Curtin<sup>2</sup>, Nicholas L. Balascio<sup>3</sup>, Raymond S. Bradley<sup>4</sup>, Dorothy M. Peteet<sup>1,5</sup>, Rafael Rapu<sup>6,7</sup>, Valenti Rull<sup>8,9</sup>, Andrea Seelenfreund<sup>10</sup>, William J. D'Andrea\*<sup>1</sup>

<sup>1</sup>*Lamont-Doherty Earth Observatory, Palisades, NY*

<sup>2</sup>*Bucknell University, Lewisburg, PA*

<sup>3</sup>*Bates College, Lewiston, ME*

<sup>4</sup>*University of Massachusetts, Amherst, MA*

<sup>5</sup>*NASA Goddard Institute for Space Studies, New York, NY*

<sup>6</sup>*Independent archeologist, Rapa Nui*

<sup>7</sup>*Universidad Católica del Norte, Chile*

<sup>8</sup>*Spanish National Research Council, Spain*

<sup>9</sup>*Catalan Institute of Paleontology, Spain*

<sup>10</sup>*Universidad Academia de Humanismo Cristiano, Chile*

*\*Corresponding Authors, [redstein@ldeo.columbia.edu](mailto:redstein@ldeo.columbia.edu); [dandrea@ldeo.columbia.edu](mailto:dandrea@ldeo.columbia.edu)*

---

This preprint on EarthArXiv has been submitted to NATURE and has not yet been peer-reviewed. If accepted, the '*Peer-Reviewed Publication DOI*' link on this webpage will be updated to direct to the final manuscript. We encourage feedback and ask that you reach out to the corresponding authors with questions and comments.

---

## ABSTRACT

From approximately 1200-1600 CE, Polynesian settlers on the island of Rapa Nui engaged in megalithic monument construction, crafting hundreds of *Ahu* platforms and *Moai* statues from volcanic bedrock. The decline of this tradition has intrigued archaeologists for decades. The most widely disseminated hypothesis surrounding the demise of the *Ahu Moai* culture suggests that the Rapanui overexploited the island's resources via slash-and-burn agriculture, leading to demographic collapse and warfare<sup>1,2</sup>. However, there is little evidence to support this claim, and genomic evidence refutes the idea of a population crash prior to European arrival<sup>3</sup>. Here, we present new evidence for a transition to drought conditions on Rapa Nui coincident with the end of the *Ahu Moai* culture, based on two independent reconstructions of hydrogen isotopes in rainfall ( $\delta^2\text{H}_{\text{precip}}$ ) inferred from hydrogen isotopes of sedimentary leaf waxes ( $\delta^2\text{H}_{\text{wax}}$ ). In accordance with observational data and model simulations, we interpret more negative  $\delta^2\text{H}_{\text{precip}}$  values to reflect an increase in the frequency of large storms and total rainfall amount over Rapa Nui. We show that the 16th-17th century decline in *Ahu* and *Moai* construction coincided with a sustained, multi-century decrease in precipitation of ~700-900 mm/year, which likely spurred territorialism over freshwater resources and instigated societal reorganization.

## INTRODUCTION

Changes in hydroclimate have been linked to major socio-political transformations globally, particularly in arid regions where freshwater availability depends strongly on precipitation<sup>4,5,6,7,8</sup>. On Rapa Nui (27.15°S, 109.4°W), surface freshwater resources are extremely limited. Despite receiving a moderate amount of rainfall (~1100 mm), local bedrock is composed of jointed basalt flows, allowing rainwater to rapidly drain through the subsurface<sup>9,10,11,12</sup>. The sole freshwater surface reservoirs on Rapa Nui are Rano Raraku lake, Rano Kao lake, and Rano Aroi wetland, all located within dormant volcanic craters (Fig. 1). Rano Aroi and Rano Raraku are prone to desiccation, however, and in recent years have dried completely. Understanding how precipitation varied in the past on Rapa Nui therefore provides critical context for understanding its human geography, including the growth and decline of megalithic architecture, as well as contemporaneous shifts in social hierarchies, spatial organization, and possible population changes in the 16th-17th century.

The timing of Polynesian arrival on Rapa Nui is contested, although most recent estimates fall between 1200-1280 CE<sup>13,14,15,16</sup>. Soon after settlement, the Rapanui people began a centuries-long tradition of building massive *Moai* statues and ceremonial *Ahu* platforms (Fig. 1), with construction likely accelerating rapidly between 1350-1450 CE<sup>14,17</sup>. Society at this time was organized into a conical clan structure, wherein the most power was held by those who could trace their ancestral lineage back to the original Polynesian settlers<sup>18,19</sup>. *Moai* statues themselves served as deified representations of ancestors, and their production by the hundreds in Rano Raraku quarry served as an organizing principle for Rapanui society<sup>1,19,20,21</sup>.

This socio-political structure transformed dramatically in the late 16th to early 17th century. Along with a decline in *Ahu* and *Moai* construction<sup>14</sup> (or, some would argue, a complete end to construction<sup>22,23,24</sup>), political representation and social hierarchies shifted, with declining prestige of the previous religious political order and the emergence of a new tradition known as Tangata Manu, where power was achieved through ritual athletic competition<sup>25,26,27</sup>. The spiritual center of the Rapanui shifted in tandem, moving from Rano Raraku crater lake, used as a quarry for *Moai* construction, to the ceremonial village of Orongo, situated on the rim of Rano Kao (Fig. 1)<sup>28</sup>. The occurrence of clan warfare during the transition between the *Ahu Moai* period and Tangata Manu is referred to as Huri Moai (Moai toppling), though evidence of direct violence or population collapse associated with Huri Moai has not been identified<sup>29,30</sup>.

To understand how freshwater availability varied through this transformative period on Rapa Nui, we measured the hydrogen isotope composition ( $\delta^2\text{H}$ ) of leaf waxes (*n*-alkanoic acids) preserved in sediments from Rano Aroi and Rano Kao (see Methods). We use these records to assess the timing and magnitude of changes in rainfall over the island and to infer associated changes in Southeast Pacific atmospheric circulation. Alkanoic acid chain-length distributions are examined to determine how changes in vegetation on Rapa Nui may have influenced the composition of leaf waxes delivered to Rano Kao and Rano Aroi (see Methods).

## DISCUSSION

### Modern $\delta^2\text{H}_{\text{precip}}$ Values on Rapa Nui Covary with Precipitation Amount

Rapa Nui is located in the remote southeast Pacific Ocean, at the juncture of three major atmospheric systems: the South Pacific Anticyclone (SPA), the South Pacific Convergence Zone (SPCZ), and the midlatitude westerlies (Appendix Fig. 1). Today the island receives ~1100 mm of rainfall per year on average, but interannual precipitation budgets are highly variable<sup>12</sup>. Total annual precipitation is determined almost entirely by the frequency of large storms (delivering > 20 mm of rainfall, after ref 29) that pass over the island, which explains 92% of the observed variance in total rainfall amount<sup>31</sup>. Seasonal changes in storm frequency over Rapa Nui are explained by the seasonality of the SPA. In austral summer, the SPA strengthens and shifts westward, blocking large storm systems associated with the midlatitude westerlies from passing over the island<sup>31,32</sup>. Recent work by Steiger et al. (2022) shows that SPA position explains 21% of the observed variance in annual rainfall from 1955 to present, and the remaining variance cannot be explained by any mode of synoptic climate variability. Other authors have argued, however, that La Niña conditions are correlated with rainfall deficits over Rapa Nui<sup>33</sup>.

We explored the relationship between  $\delta^2\text{H}_{\text{precip}}$  and precipitation amount over Rapa Nui using monthly measurements of stable isotopes in rainfall, available from 1991-2018 (n = 317) through the Global Network of Isotopes in Precipitation (GNIP)<sup>34</sup>. Annual precipitation-weighted  $\delta^2\text{H}_{\text{precip}}$  in this dataset has a significant negative correlation with mean annual precipitation (R = -0.52, p = .008) (Fig. 2A) and with the annual frequency of large storms, (R = -0.55 and p = 0.004) (Fig. 2B), while showing an insignificant relationship to annual mean temperature and vapor pressure (Appendix Fig. 2). The equation describing the relationship between rainfall amount and  $\delta^2\text{H}_{\text{precip}}$  values is:

$$\delta^2 H_{\text{Annual precip}} = -0.0117 X_{\text{MAP}} + 8.41 \quad (1)$$

where  $X_{\text{MAP}}$  is equal to the mean annual precipitation in millimeters.

On a monthly basis,  $\delta^2\text{H}_{\text{precip}}$  values do not show a statistically significant correlation with rainfall amount or large storm (>20 mm) frequency. However, months with fewer large storms do have more positive  $\delta^2\text{H}_{\text{precip}}$  values on average. With increasing large storm frequency, monthly  $\delta^2\text{H}_{\text{precip}}$  values decrease and converge towards a mean of approximately -20‰ (VSMOW), and the range

of observed  $\delta^2\text{H}_{\text{precip}}$  values decreases in tandem (Appendix Fig. 3). This may indicate that precipitation associated with large storm systems has a consistently more negative isotopic signature, while precipitation associated with smaller rainfall events may have more variable isotopic composition, attributable to changing source region, relative humidity during rainout, or varying degrees of Rayleigh distillation<sup>35</sup>. On longer timescales (1871-2011), ECHAM5-wiso model simulations suggest that monthly  $\delta^2\text{H}_{\text{precip}}$  values over Rapa Nui and the surrounding region have a highly significant, negative correlation with regional precipitation amount (Fig. 2C), and a significant positive relationship with easterly wind velocity and sea level pressure associated with SPA circulation (Appendix Fig. 4)<sup>36</sup>.

### **$\delta^2\text{H}_{\text{wax}}$ in Rano Aroi and Rano Kao Reflects $\delta^2\text{H}_{\text{precip}}$**

Long chain *n*-alkanoic acids record the isotopic composition of amount-weighted source water during their growing season<sup>35</sup>. On Rapa Nui, where plant growth is not seasonally restricted, we expect leaf waxes to record the mean annual  $\delta^2\text{H}$  value of source water. Rano Kao is a rainwater-fed, closed-basin lake with no outflow. In Rano Kao, samples were extracted from a floating mat of totora (*Schoenoplectus californicus*), which sources water directly from the surrounding lake. Rano Kao lake water  $\delta^2\text{H}$  values are determined by the hydrogen isotope composition of incoming precipitation ( $\delta^2\text{H}_{\text{precip}}$ ) and by evaporative fractionation. We expect these processes to be complementary. Intervals with fewer large storms would have more positive  $\delta^2\text{H}_{\text{precip}}$  (see Equation 1) and greater evaporation would also result in more positive lake water  $\delta^2\text{H}$  values. Plants in Rano Aroi on Terevaka peak (430m) receive moisture from a combination of precipitation and groundwater<sup>10</sup>. Given that rainwater rapidly percolates through the subsurface on Rapa Nui, we anticipate relatively little post-depositional fractionation of hydrogen in rainwater during recharge of the main aquifer. This is supported by previous isotopic surveys ( $\delta^2\text{H}$ ,  $\delta^{18}\text{O}$ ) on Rapa Nui, which show minimal offset between meteoric, borehole, and well water<sup>10</sup>. Thus,  $\delta^2\text{H}_{\text{wax}}$  values in wetland plants likely reflect a multi-year integration of  $\delta^2\text{H}_{\text{precip}}$  from groundwater, superimposed with higher frequency variability imparted from rainfall  $\delta^2\text{H}_{\text{precip}}$ . We therefore interpret  $\delta^2\text{H}_{\text{wax}}$  from Rano Aroi to represent  $\delta^2\text{H}_{\text{precip}}$  and thereby precipitation amount on Rapa Nui (Equ. 1). We interpret  $\delta^2\text{H}_{\text{wax}}$  from Rano Kao to reflect  $\delta^2\text{H}_{\text{precip}}$ , compounded with the effect of evaporative fractionation on lake water.

### **$\delta^2\text{H}_{\text{wax}}$ Values Reveal 16th Century Drought on Rapa Nui:**

In both the Rano Aroi and Rano Kao records,  $\delta^2\text{H}_{\text{wax}}$  of  $\text{C}_{26}$  and  $\text{C}_{28}$  alkanolic acids show strong covariability (Fig. 3).  $\delta^2\text{H}_{\text{wax}}$  values in Rano Kao are more positive than those in Rano Aroi, likely due to the evaporative fractionation of Rano Kao water and differences in altitude between the sites. At approximately 1200 CE in Rano Aroi,  $\delta^2\text{H}_{\text{wax}}$  values began gradually decreasing, reaching a minimum at 1300 CE of -153.9‰ for  $\text{C}_{28}$  and -150.7‰ for  $\text{C}_{26}$ . From 1300-1850 CE,  $\delta^2\text{H}_{\text{wax}}$  gradually increased by approximately 17‰ for  $\text{C}_{28}$  and 13‰ for  $\text{C}_{26}$ , showing the largest step change between 1500-1560 CE of 7.7‰ and 6.6‰ respectively. In the Rano Kao record,  $\delta^2\text{H}_{\text{wax}}$  values reach a minimum later than in Rano Aroi, c. 1470 CE. Coincident with the positive  $\delta^2\text{H}_{\text{wax}}$  excursions observed in Rano Aroi,  $\delta^2\text{H}_{\text{wax}}$  values in Rano Kao sharply increased by 15-20‰ at approximately 1550 CE. Higher  $\delta^2\text{H}_{\text{wax}}$  values persisted until the top of the Rano Kao sedimentary record, c. 1710 CE. We interpret the increase in  $\delta^2\text{H}_{\text{wax}}$  at ~1550 CE in both records as an increase in  $\delta^2\text{H}_{\text{precip}}$  over Rapa Nui, and thus a sustained decrease in regional precipitation.

We reject the possibility that observed changes in  $\delta^2\text{H}_{\text{wax}}$  are attributable to vegetation changes. To determine whether shifts in terrestrial vegetation on Rapa Nui (e.g. palm clearance) influenced the sources of *n*-alkanoic acids delivered to the Rano Aroi and Rano Kao, we calculated average chain lengths for long-chain ( $\text{C}_{26}$ - $\text{C}_{32}$ ) sedimentary *n*-alkanoic acids ( $\text{ACL}_{26-32}$ ) (Methods). In Rano Aroi,  $\text{ACL}_{26-32}$  shows virtually no change across the period of local palm deforestation (~1520-1620 CE) (Appendix Fig. 5C)<sup>38</sup>. Additionally, carbon isotope measurements do not support a significant shift in C3/C4 plant distribution around Rano Aroi from at least ~1250 CE to European arrival<sup>38</sup>. In Rano Kao, there is similarly no change in  $\text{ACL}_{26-32}$  across the interval of palm clearance (~1350-1800 CE)<sup>39</sup> (Appendix Fig. 5C). Given the lack of stream inflow into the caldera and its steep, high walls, it is likely that long-chain leaf waxes in the floating mats of Rano Kao were produced almost entirely by wetland vegetation. For both sites, we therefore assume that leaf wax apparent fractionation ( $\epsilon_{\text{wax-water}}$ ) is constant prior to 1722 CE. We apply a  $\epsilon_{\text{wax-water}}$  value of -99‰, consistent with global averages<sup>37,40</sup>.

Changes in  $\delta^2\text{H}_{\text{wax}}$  may not be reliable indicators of underlying changes in  $\delta^2\text{H}_{\text{precip}}$  following European arrival (1722 CE), and particularly following Chilean annexation of Rapa Nui (1888 CE<sup>41,42</sup>).  $\text{ACL}_{26-32}$  values in Rano Aroi show higher variability after 1722 CE and decrease

significantly after 1890 CE, coinciding with an abrupt decrease in  $\delta^2\text{H}_{\text{wax}}$  values ( $>20\%$ ) and marked changes in sedimentology (Appendix Figure 6). These changes align with the advent of intensive sheep farming on the island ( $\sim 1903\text{-}1953$  CE) and the introduction of non-native plant species (e.g. *Eucalyptus*)<sup>41,42</sup>.

In Rano Aroi, mean  $\delta^2\text{H}_{\text{wax}}$  values for the 1550-1720 CE period were 8.2‰ and 10.6‰ higher for  $\text{C}_{26}$  and  $\text{C}_{28}$  leaf-waxes respectively compared to the 1200-1550 CE period. This earlier interval broadly aligns with the timing of peak *Ahu* and *Moai* construction on Rapa Nui, while the later interval overlaps with the emergence and growth of Tangata Manu, prior to European Arrival (1722 CE). Averaging these  $\delta^2\text{H}_{\text{wax}}$  values for  $\text{C}_{26}$  and  $\text{C}_{28}$  alkanolic acids, our record suggests that  $\delta^2\text{H}_{\text{precip}}$  values over Rapa Nui were  $\sim 10\%$  higher for the 1550-1720 CE period relative to 1200-1550 CE, corresponding to a precipitation deficit of  $\sim 890$  mm per year (Equ. 1). In Rano Kao, mean  $\delta^2\text{H}_{\text{wax}}$  values for the 1550-1710 CE period were 8.2‰ and 7.4‰ higher for  $\text{C}_{26}$  and  $\text{C}_{28}$  leaf-waxes respectively compared to the 1200-1550 CE period. Applying the same calculations as in Rano Aroi, we calculate a precipitation deficit of  $\sim 740$  mm per year, though we note that  $\delta^2\text{H}_{\text{source water}}$  in this case is lake water subject to evaporative isotope fractionation.

For context, a recent interval of drought on Rapa Nui (2010-2017), which put significant stress on local freshwater reserves and led to the drying of Rano Raraku<sup>43</sup>, was associated with a mean reduction in annual precipitation of  $\sim 370$  mm per year relative to the prior two decades in the Global Network of Isotopes in Precipitation dataset (Appendix Fig. 7). A reduction in annual rainfall on the order of  $\sim 700\text{-}900$  mm would have represented a significant shift in local hydroclimate and posed challenges to the Rapanui.

The timing of this inferred drought at  $\sim 1550$  CE aligns with a hiatus in the Rano Raraku record (1550-1720 CE)<sup>44</sup>, as well as geochemical indicators of sediment oxidation in Rano Aroi<sup>45</sup>, both previously proposed to reflect drying. However, whereas there can be multiple, complex drivers of changes in wetland geochemistry and sediment accumulation rates, our record explicitly records paleoprecipitation variability on Rapa Nui and, based on model simulations, further suggests that drought was driven by a stronger South Pacific Anticyclone (Appendix Fig. 4) that blocked

approaching storm systems. It is challenging to attribute a strengthening and/or shift in SPA position during the 16th-18th century to a single cause, particularly given that the mean state of the tropical Pacific during this time period is unconstrained. However, a strengthened SPA during the 16th-18th century is consistent with numerous proxy records of precipitation from South America, which indicate an enhanced summer monsoon<sup>46,47,48</sup>. Upper-level divergence associated with monsoonal heating over South America contributes significantly to SPA strength by increasing subsidence to the west of the continent, leading to a region of high-pressure via the Rodwell-Hoskins mechanism<sup>49</sup>.

### **Influence of Drought on Rapanui Society**

There is evidence that the Rapanui dealt with freshwater scarcity from the time of their arrival. While crater lakes, and in particular Rano Kao, were likely relied upon for drinking water to some extent<sup>50</sup>, recent studies suggest that coastal groundwater discharge was a primary source of drinking water<sup>11,51,52</sup>. The location of *Ahu* platforms is closely linked to coastal groundwater sources (Fig. 1), which enabled clans to disperse across the island<sup>52</sup>. The *Ahu* themselves are thought to have delineated community control over these limited freshwater resources<sup>52</sup>. The Rapanui also engaged in a variety of freshwater management techniques, including rainwater harvesting in carved *taheta* basins and the construction of coastal cisterns known as *puna*<sup>9,11,53,54</sup>. Specialized agricultural techniques, such as lithic mulching, were employed to minimize evaporative moisture loss from soils, which are excessively drained<sup>55,56</sup>.

Although the Rapanui were equipped to deal with limited freshwater resources and likely resilient to temporary reductions in rainfall, at approximately 1550 CE, a multi-century precipitation deficit led to the sustained drying of Rano Raraku lake and limited the amount of rainwater that could be collected in *taheta*. Initially, this drought may have pushed islanders to rely more heavily on coastal groundwater discharge, as theorized by Brosnan et al. (2018)<sup>11</sup>. Thermal imaging surveys conducted in 2019, following recent multi-year drought (2010-2018), indicated that while Rano Raraku and Rano Aroi quickly dried out, coastal groundwater discharge remained abundant due to the relatively long turnover time (10-50 years) of the island's main groundwater aquifer<sup>10,11,51</sup>. Importantly, however, our reconstructed drought was more severe than that of recent years and persisted for well over a century. Therefore, it is plausible that after an initial phase of drought c.

1550 CE pushed islanders to more heavily rely on coastal groundwater discharge, a reduction in flow rate eventually reduced the potability of these waters for human consumption. Spatially inconsistent reductions in the coastal groundwater outflow, and thus water quality, further provides a plausible reason for heightened tensions (or conflict) between clans, including the toppling of Moai to dispute ownership over seep sites, or abandonment and decay of Moai overlooking certain seeps.

Our work suggests that freshwater availability had a role in shaping community geographies on Rapa Nui, likely due to imparted variability on the drying of lakes, the potability of coastal seep water, and perhaps agricultural production by reducing soil moisture. Our hypothesis does not necessitate violent war or demographic collapse at 1600 CE, but provides a reasonable explanation for possible drivers of intercommunity conflict, a need for spatial reorganization, and an impetus for cultural development on the island. More broadly, our work underscores the importance of understanding the climatic backdrop for past socio-political transformations, particularly in regions where freshwater resources are scarce.

## FIGURES

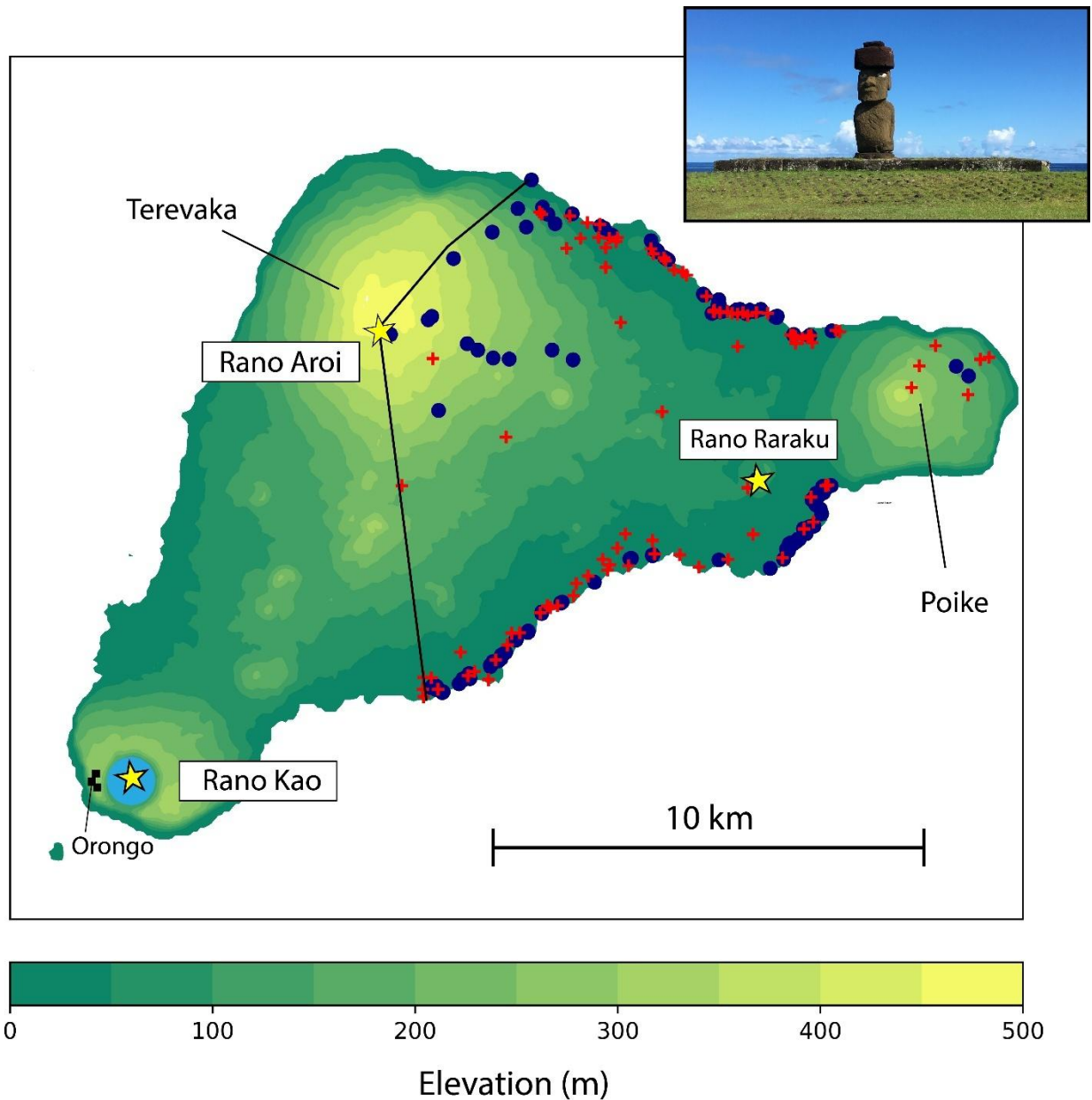


**Figure 1:** Digital elevation model of Rapa Nui (27.15°S, 109.4°W), from NOAA’s National Center for Environmental Information. Permanent lakes and wetlands, including Rano Kao, Rano Raraku, and Rano Aroi, are starred and labelled. Other freshwater sources, including springs, ponds, caves with seeping groundwater, *puna*, and coastal groundwater discharge, are marked by navy circles. These sites were identified and mapped by DiNapoli et al. (2019) within the eastern sector of the island, bounded by solid black lines<sup>52</sup>. The locations of *Ahu* platforms within this study area are marked with red crosses. A photo of an *Ahu* platform and single *Moai* statue is shown in the upper right corner.

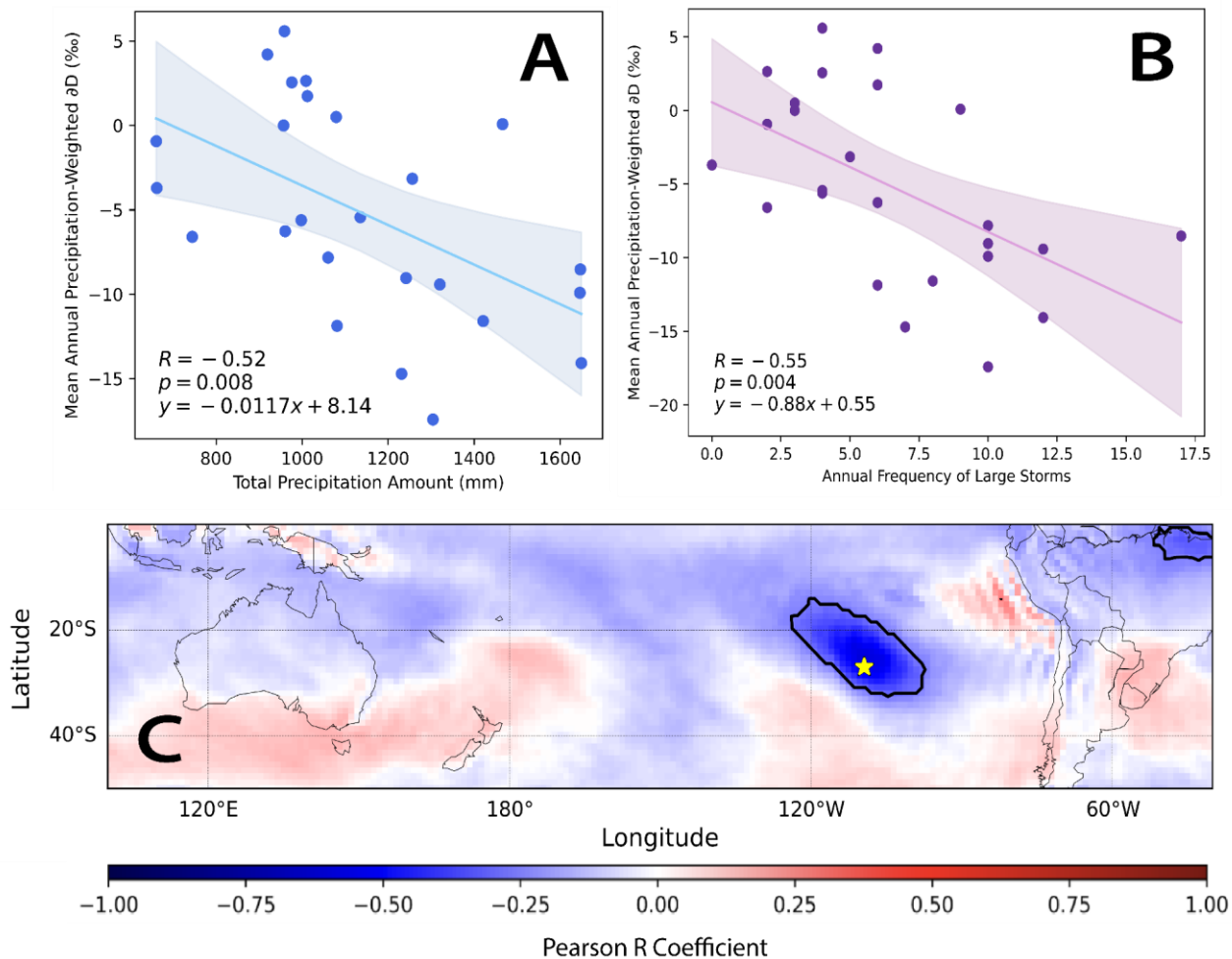


**Figure 2:** [A] Annual precipitation amount and [B] annual frequency of large storms (>20mm) compared with annual amount-weighted  $\delta^2\text{H}_{\text{precip}}$  calculated from monthly data from the Global Network of Isotopes in Precipitation (GNIP) station on Rapa Nui. Years with <10 months of available  $\delta^2\text{H}_{\text{precip}}$  data were excluded from the dataset. [C] Pearson regression coefficients for monthly ECHAM5-wiso simulated  $\delta^2\text{H}_{\text{precip}}$  values over Rapa Nui (1871-2011) and the surrounding region ( $7^\circ \times 7^\circ$  grid centered on Rapa Nui grid cell) compared against the simulated total precipitation values over the SH Pacific. Black contours represent a significance level of  $p < 1e-24$ . The location of Rapa Nui is starred.

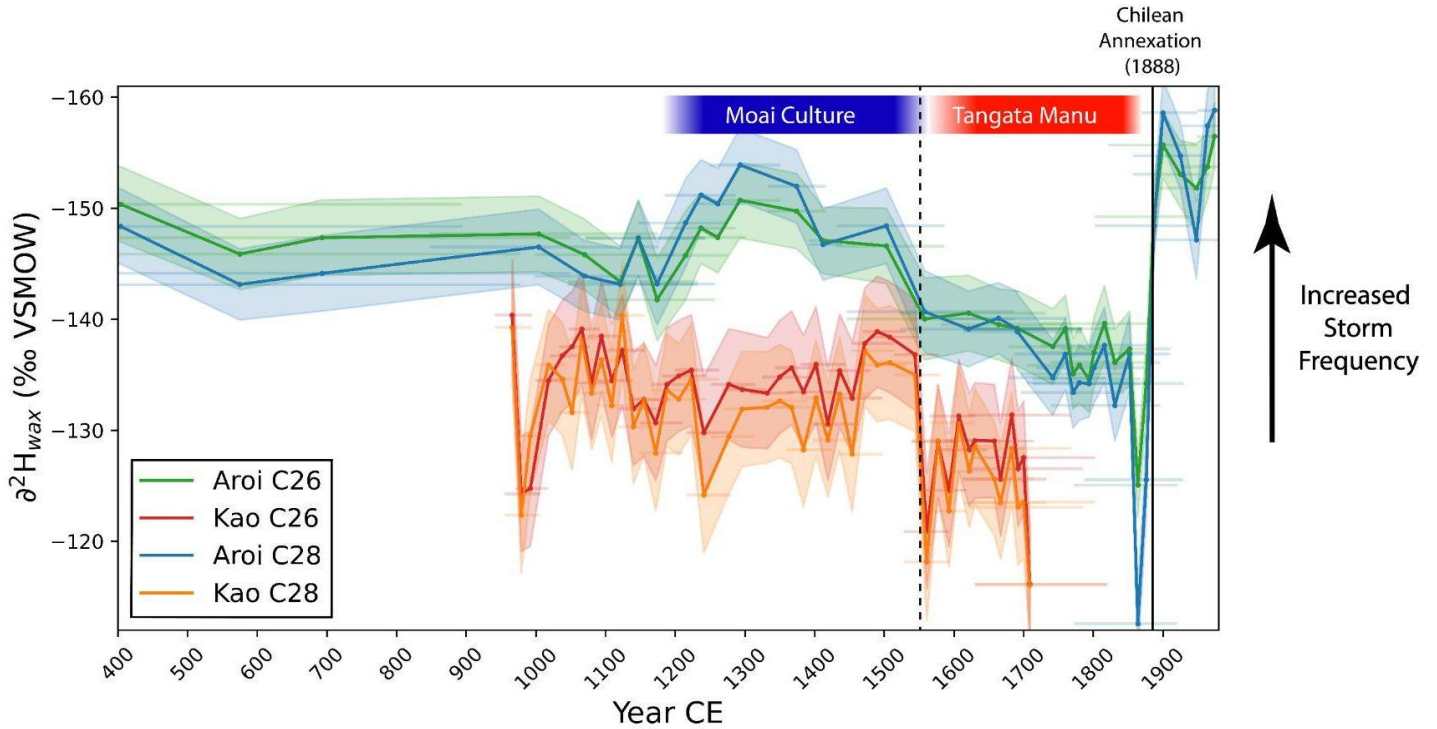


**Figure 3:** Leaf wax (*n*-alkanoic acid) hydrogen isotope values through time from Rano Aroi and Rano Kao. Results from C<sub>28</sub> and C<sub>26</sub> *n*-alkanoic acids are shown for both sites. Uncertainty in  $\delta^2\text{H}_{\text{wax}}$  represents the standard error of the mean. Uncertainty in the age represents the 95% confidence interval for the sample age, calculated using Bacon (Appendix Fig. 8) for Rano Aroi and Clam R 2.2 for Rano Kao<sup>21</sup>. Note that the y-axis is inverted such that wetter conditions (more frequent large storms) are in the up direction.

## METHODS

**Hydrogen Isotopes of Precipitation:** The isotopic composition of hydrogen in precipitation is influenced by aspects of large-scale atmospheric dynamics and regional climate<sup>35</sup> and is expressed in delta notation relative to a standard (*Vienna Standard Mean Ocean Water*; VSMOW) according to the equation:

$$\delta^2H_{precip} = \left( \frac{{}^2H/H_{sample}}{{}^2H/H_{VSMOW}} - 1 \right) * 1000 \quad (2)$$

The  $\delta^2H$  value of leaf waxes reflects the  $\delta^2H$  value of plant source water, with particularly high fidelity in dry regions<sup>37</sup>. In semiarid, subtropical climates that experience large, infrequent rainfall events, large storms deliver precipitation that is relatively depleted in  ${}^2H$  (i.e. with a more negative  $\delta^2H$  value) and this isotopic signature is imparted into soil moisture<sup>57</sup>. Wetland sediments from Rapa Nui preserve an archive of leaf wax  $\delta^2H$  values, thus recording regional hydroclimate variability through time. Here, we analyze two sediment cores: RAP-01-18 D1 from Rano Aroi wetland, and KAO08-03 from a floating mat of totora in Rano Kao.

**Sample Collection:** Core KAO08-03 was collected from a floating mat in Rano Kao crater lake in 2008 using a Russian peat corer. The entire sequence of the mat was taken in five drives, extending to a depth of 300 cm<sup>21</sup>. Core RAP-01-18 was collected from Rano Aroi wetland in 2018 using a modified Nesje corer. Sediment was retrieved near the edge of the mire, close to the location of ARO 08 02, previously studied by Margalef et al. (2013)<sup>58</sup>. The entire core was taken in four drives and extends to ~420 cm. Only samples from Drive 1 (154cm) are presented in this study. Sediments were refrigerated after collection and transported and stored in cold storage at the Lamont-Doherty Earth Observatory.

**Quantifying *n*-Alkanoic Acid  $\delta^2H_{wax}$  Values:** Samples of 1 cm thickness were collected at 5 cm intervals from sediment core RAP-01-18 D1 from Rano Aroi mire, collected in 2018, and core KAO08-03. Additional sub-samples were taken across intervals with more rapid sediment accumulation, as determined by the  ${}^{14}C$ -based age-depth models, in order to achieve consistent temporal sampling resolution where possible. Sediments were freeze dried and homogenized. Free lipids were extracted from each sample using a Dionex Accelerated Solvent Extractor (ASE 350) with a 9:1 v/v mixture of dichloromethane:methanol. Total lipid extracts (TLEs) were spiked with an internal standard mixture and split into an archive and a working half. The working sample was

filtered over ashed glass wool to remove large particles, dried down under N<sub>2</sub> gas, and brought up in ~ 0.5mL of 2:1 dichloromethane:isopropanol. To isolate neutral, acidic, and polar compounds respectively, TLEs were loaded onto a solvent-rinsed aminopropyl gel column and eluted with four bed volumes each of 2:1 dichloromethane:isopropanol, 4% acetic acid in ethyl ether, and methanol. The acid fraction containing *n*-alkanoic acids was then dried down, brought up in acetyl chloride-acidified methanol, and heated at 60°C for 2 hours in order to induce methylation. To track the isotopic composition of the added methyl group, a 100uL sample of phthalic acid standard of a known isotopic composition (-95.5 ±2.2‰) was methylated using the same procedure. Fatty acid methyl esters (FAMES) were then recovered from each sample using three liquid-liquid separations with 5:1 hexane:dichloromethane. FAMES were further purified using silica gel chromatography, then transferred to 2mL vials and brought up in ~500uL of hexane for identification and quantification using Gas Chromatography Mass Selective Detection (GC-MSD) and compound-specific hydrogen isotope analysis using Gas Chromatography Isotope Ratio Mass Spectroscopy (GC-IRMS).

Hydrogen isotope compositions were measured in triplicate for chain lengths C<sub>16</sub>-C<sub>32</sub> using a Thermo Trace GC-IRMS. 1-3uL of each sample was injected into a PTV inlet in splitless mode at 60°C and rapidly heated to 320°C before being vented onto the column using a helium (He) carrier gas. Oven temperature was held at 60°C for 90 seconds, then ramped at 15°C/min to 150°C and again at 4°C/min to 320°C before being held for 10 minutes. Isotopic compositions were adjusted to the VSMOW scale and further corrected using the phthalic acid standard to account for the hydrogen isotope composition of the added methyl using the method described by Polissar & D'Andrea (2014)<sup>59</sup>. Samples with peak areas <10 Vs and >150 Vs were not used.

**Quantifying *n*-Alkanoic Acid Chain Length Distributions:** C<sub>16</sub>-C<sub>32</sub> *n*-alkanoic acids were quantified using an Agilent 5890 gas chromatograph coupled to an Agilent 7890A mass selective detector. 1-3uL of each sample was injected into a multimode inlet in PTV mode at 60°C, then rapidly heated to 320°C and transferred onto the GC column using He gas. The oven was held at 60°C for 90 seconds, ramped to 150°C at 14°C/min, then ramped at 4°C/min to 320°C and held for 25 minutes. Resulting chromatogram peaks for each chain length were quantified using mass ion 71. Response factors for each chain length were calculated relative to C<sub>26</sub> *n*-alkanoic acid using an

external FAME standard with known molecular concentrations, which was run every 5-6 samples. These response factors were then used to quantify chain-length abundance for sample  $n$ -alkanoic acids. Relative concentrations of each chain length were calculated by dividing the integrated ion response by the response factor.

Average chain-lengths were calculated across a variety of ranges ( $i = 20, 24, 26$ ) using the following equation, where  $n$  indicates chain length, and  $C_n$  indicates chain length abundance:

$$ACL = \frac{\sum_i^{32} (C_n * n)}{\sum_i^{32} (C_n)} \quad (3)$$

$ACL_{26-32}$  is shown in Appendix Figure 5.

### **Isolation of Terrestrial Macrofossils and Pollen Extracts**

To extract macrofossils, 1 cm-wide subsamples (5-8 ccs) were removed from the Rano Aroi sediment core using a clean spatula and filtered over a 125 $\mu$ m sieve to remove clays and small organic particles. Terrestrial plant material (e.g. seeds, bark, leaves) was identified under a stereomicroscope and transferred to a 4mL vial. Samples were then freeze dried and sent to the University of California Irvine Keck Facility for AMS C-14 dating. Pollen samples were extracted for parts of the sediment core with no identifiable terrestrial plant material in the >125 $\mu$ m sieved fraction following a procedure modified from Vandergoes and Prior, 2003<sup>60</sup>. To generate pollen extracts, 5-8cc of sediment were boiled in 10% KOH solution for 10 minutes, then filtered through a 125 $\mu$ m and 7 $\mu$ m sieve using deionized (DI) water, discarding the fractions >125 $\mu$ m and <7 $\mu$ m. The sample was then centrifuged at ~3000 RPM for 10 minutes and the DI water decanted. A 10% HNO<sub>3</sub> solution was then added to each centrifuge tube and allowed to sit for 3-5 minutes to break up organic material. Samples were then centrifuged and decanted three times, rinsing with deionized water each time to remove any residual HNO<sub>3</sub>. Density separations were performed using heavy liquid (polytungstate) with a density range of 1.2-1.35 SPT. Samples were rinsed once more with DI water, centrifuged, and transferred to 4mL vials. A subset of samples were analyzed under 400x magnification to confirm the presence of pollen. Extracts were then freeze dried and sent for AMS C-14 dating at the UC Irvine Keck Facility.

**Age Modeling in BACON:** An age model was constructed using the software Bacon<sup>62</sup>. Radiocarbon ages were converted to calendar age using the southern hemisphere SHcal20 calibration curve. For samples dated to the post-bomb period (1950 - present), D<sup>14</sup>C values were used to estimate a calendar age, using the CALIBomb software and the SH Zone 1-2 calibration dataset<sup>64</sup>. Priors including memory strength (4), memory mean (0.7), accumulation shape (2), and accumulation mean (135) were chosen in accordance with previous age models of Rano Aroi<sup>58,62</sup>. Sediment thickness was set to 4cm, to allow for a slightly higher degree of smoothing relative to the default of 5cm. Ages and associated errors from Rano Kao are taken from a published age model in Rull et al., 2018, which uses Clam.R 2.2 with smooth spline interpolation<sup>21</sup>.

**GNIP and ECHAM5-wiso Analysis:** Monthly measurements of hydrogen isotopes in precipitation over Rapa Nui (n = 317) were taken by the Global Network of Isotopes in Precipitation (GNIP) from 1991-2018. These data were downloaded from GNIP's open-source, online database. For analysis of annual precipitation-weighted  $\delta^2\text{H}_{\text{precip}}$  values, missing months in the dataset were ignored. Rho values, Pearson correlation coefficients, confidence intervals, and linear regressions between variables were calculated using the Scipy.stats package in Python.

Monthly ECHAM5-wiso model simulation data for the period 1871-2011 were downloaded from Zenodo repository associated with Steiger et al., 2018<sup>36</sup>. Boundary conditions were interpolated HadISST fields. The model was run at 1 degree resolution. In order to investigate correlations between hydrogen isotopes in precipitation over Rapa Nui and regional climate variables,  $\delta^2\text{H}_{\text{precip}}$  values and monthly precipitation amounts were extracted from a 7° x 7° grid, centered on Rapa Nui. A single  $\delta^2\text{H}_{\text{precip}}$  value was calculated for the region as a precipitation amount-weighted mean of each individual gridcell. Pearson R correlation coefficients were calculated between these monthly  $\delta^2\text{H}_{\text{precip}}$  values and total monthly precipitation amounts (Fig. 2C), 10m wind speeds (Appendix Fig. 4A), and sea level pressure (Appendix Fig. 4B) for all other grid cells for the 1871-2011 time period, again using Scipy.stats.

**Acknowledgements:** We would like to thank the Ma'u Henua Indigenous Community and the Chilean National Forestry Service (CONAF) for permitting and logistically supporting field work on Rapa Nui conducted for this study, as well as the Rapa Nui Office of the Secretaría Técnica de

Patrimonio at the Consejo de Monumentos Nacionales for permission to excavate and export sediment cores. Excavation permit was granted under permit 6214 (27-12. 2017) and permission to export sediment cores to the USA under permit 2869 (04.07.2018). We would like to acknowledge the support of the National Science Foundation award EAR-1903676 to WJD and the William & Mary Reves Faculty Fellowship to NLB. We additionally thank the Vetlesen Foundation and Explorer's Club for funding provided to WJD and LC respectively. We thank Helen Habicht, Wei Huang, Sachi Thomson, and Tyler Clemens for their assistance in the lab, and James Van Hook for his assistance with field work.

**Author Contributions:** W.J.D. conceived of the study project and oversaw activities relating to research, including field work, lab work, and writing. R.S. conducted laboratory work, data analysis, and wrote the manuscript. N.B., R.B., and L.C. helped conceive of this project, conducted field work, and contributed to writing the manuscript. D.P. provided laboratory facilities and oversight of macrofossil identification, assisted with pollen extraction for the Rano Aroi age model, and edited the manuscript. V.R. provided sediment for the Rano Kao record and contributed to writing the manuscript. R.R. and A.S. oversaw field work on Rapa Nui and provided guidance on archeological interpretations. Correspondence should be addressed to R.S and W.J.D.

## REFERENCES

1. Flenley, J. & Bahn, P. G. *The Enigmas of Easter Island: Island on the Edge*. (Oxford University Press, Oxford ; New York, 2003).
2. Jared Diamond. *Collapse: How Societies Choose to Fail or Succeed: Revised Edition*. (Penguin Books, New York, 2011).
3. Moreno-Mayar, J. V. *et al.* Ancient Rapanui genomes reveal resilience and pre-European contact with the Americas. *Nature* 633, 389–397 (2024).
4. Zheng, J. *et al.* How climate change impacted the collapse of the Ming dynasty. *Climatic Change* 127, 169–182 (2014).
5. Zhang, H. *et al.* Collapse of the Liangzhu and other Neolithic cultures in the lower Yangtze region in response to climate change. *Science Advances* 7, eabi9275 (2021).
6. Ren, M. *et al.* The collapse of the Ming Dynasty actually began with the Wanli megadrought: Insights from a hydroclimate reconstruction based on tree-ring  $\delta^{18}\text{O}$  over the past 460 years. *Palaeogeography, Palaeoclimatology, Palaeoecology* 655, 112548 (2024).
7. Cullen, H. M. *et al.* Climate change and the collapse of the Akkadian empire: Evidence from the deep sea. *Geology* 28, 379–382 (2000).
8. deMenocal, P. B. Cultural Responses to Climate Change During the Late Holocene. *Science* 292, 667–673 (2001).
9. Hixon, S. W., DiNapoli, R. J., Lipo, C. P. & Hunt, T. L. The Ethnohistory of Freshwater Use on Rapa Nui (Easter Island, Chile). *The Journal of the Polynesian Society* 128, 163–190 (2019).1.
10. Herrera, C. & Custodio, E. Conceptual hydrogeological model of volcanic Easter Island (Chile) after chemical and isotopic surveys. *Hydrogeology Journal* 16, 1329–1348 (2008).
11. Brosnan, T., Becker, M. & Lipo, C. Coastal groundwater discharge and the ancient inhabitants of Rapa Nui (Easter Island), Chile. *Hydrogeology Journal* 27, (2018).
12. Bradley, R. S., D'Andrea, W. J., Diaz, H. F. & Ning, L. Climatology of Rapa Nui (Isla de Pascua, Easter Island). in *The Prehistory of Rapa Nui (Easter Island): Towards an Integrative Interdisciplinary Framework* (eds. Rull, V. & Stevenson, C.) 259–274 (Springer International Publishing, Cham, 2022). doi:[10.1007/978-3-030-91127-0\\_11](https://doi.org/10.1007/978-3-030-91127-0_11).
13. Schmid, M. M. E. *et al.* How  $^{14}\text{C}$  dates on wood charcoal increase precision when dating colonization: The examples of Iceland and Polynesia. *Quaternary Geochronology* 48, 64–71 (2018).

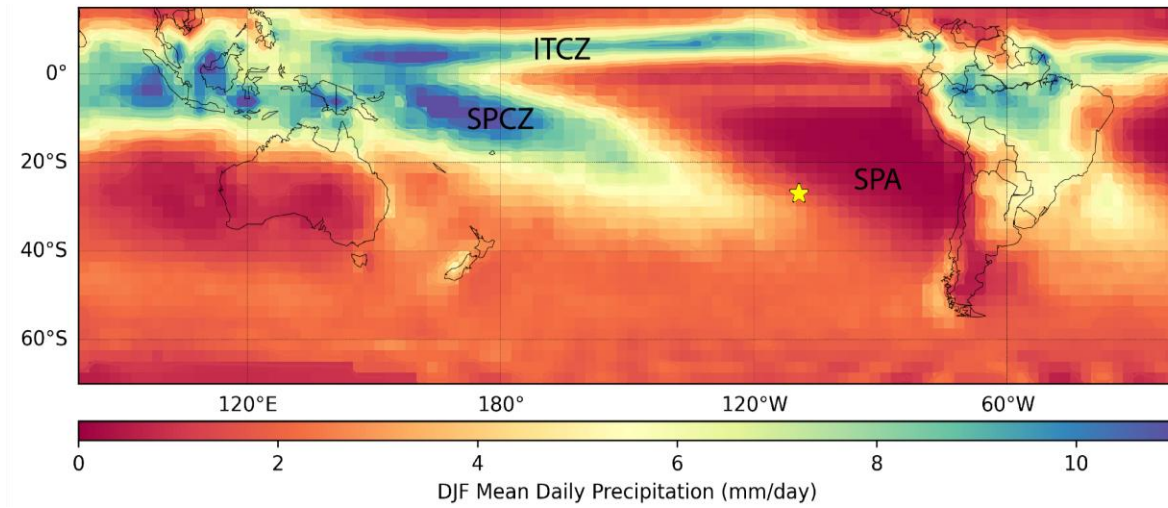
14. DiNapoli, R. J., Rieth, T. M., Lipo, C. P. & Hunt, T. L. A model-based approach to the tempo of “collapse”: The case of Rapa Nui (Easter Island). *Journal of Archaeological Science* **116**, 105094 (2020).
15. Hunt, T. L. & Lipo, C. P. Late Colonization of Easter Island. *Science* **311**, 1603–1606 (2006).
16. Mann, D. *et al.* Drought, vegetation change, and human history on Rapa Nui (Isla de Pascua, Easter Island). *Quaternary Research* **69**, 16–28 (2008).
17. Martinsson-Wallin, H., Wallin, P., Anderson, A. & Solsvik, R. Chronogeographic Variation in Initial East Polynesian Construction of Monumental Ceremonial Sites. *Journal of Island & Coastal Archaeology* **8**, 405–421 (2013).
18. Tilburg, V. & Anne, J. Easter Island. in *Encyclopedia of Prehistory* 45–59 (Springer, Boston, MA, 2001). doi:[10.1007/978-1-4615-1189-2\\_8](https://doi.org/10.1007/978-1-4615-1189-2_8).
19. Richards, C. *et al.* Road my body goes: re-creating ancestors from stone at the great moai quarry of Rano Raraku, Rapa Nui (Easter Island). *World Archaeology* **43**, 191–210 (2011).
20. Edwards E. *et al.* When the Universe was an island: exploring the cultural and spiritual Cosmos of Ancient Rapa Nui. *Hangaroa: Hangaroa Press* (2013).
21. Rull, V. *et al.* CLAFS, a Holistic Climatic-Ecological-Anthropogenic Hypothesis on Easter Island’s Deforestation and Cultural Change: Proposals and Testing Prospects. *Front. Ecol. Evol.* **6**, (2018).
22. Martinsson-Wallin, H., Wallin, P., Anderson, A. & Solsvik, R. Chronogeographic Variation in Initial East Polynesian Construction of Monumental Ceremonial Sites. *Journal of Island & Coastal Archaeology* **8**, 405–421 (2013).
23. Conrich, I. & Mückler, H. *Rapa Nui – Easter Island: Cultural and Historical Perspectives*. (Frank & Timme GmbH, 2016).
24. Hamilton, S., Thomas, M. S. & Whitehouse, R. Say it with stone: constructing with stones on Easter Island. *World Archaeology* **43**, 167–190 (2011).
25. Robinson, T. & Stevenson, C. M. The Cult of the Birdman: Religious Change at ‘Orongo, Rapa Nui (Easter Island). *Journal of Pacific Archaeology* **8**, 88–102 (2017).
26. Lee, G. & Liller, W. Easter Island’s “Sun Stones”: A Re-Evaluation. *Journal for the History of Astronomy* **18**, S1–S11 (1987).
27. Rull, V. Natural and anthropogenic drivers of cultural change on Easter Island: Review and new insights. *Quaternary Science Reviews* **150**, 31–41 (2016).

28. Kirch, P. V. *On the Road of the Winds: An Archaeological History of the Pacific Islands Before European Contact, Revised and Expanded Edition*. (Univ of California Press, 2017).
29. Lipo, C. P., Hunt, T. L., Horneman, R. & Bonhomme, V. Weapons of war? Rapa Nui mata'a morphometric analyses. *Antiquity* **90**, 172–187 (2016).
30. Hunt, T. & Lipo, C. *The Statues That Walked: Unraveling the Mystery of Easter Island*. (Simon and Schuster, 2011)
31. Steiger, N. J., D'Andrea, W. J., Smerdon, J. E. & Bradley, R. S. Large infrequent rain events dominate the hydroclimate of Rapa Nui (Easter Island). *Clim Dyn* **59**, 595–608 (2022).
32. Seager, R. *et al.* Air–Sea Interaction and the Seasonal Cycle of the Subtropical Anticyclones. *Journal of Climate* **16**, 1948–1966 (2003).
33. Delcroix, T. *et al.* Clarifying the Role of ENSO on Easter Island Precipitation Changes: Potential Environmental Implications for the Last Millennium. *Paleoceanography and Paleoclimatology* **37**, e2022PA004514 (2022).
34. IAEA/WMO (2024). Global Network of Isotopes in Precipitation. The GNIP Database. Accessible at: <https://nucleus.iaea.org/wiser>
35. Sharp, Z. Principles of Stable Isotope Geochemistry, 2nd Edition. *Open Textbooks* (2017) doi:<p><https://doi.org/10.25844/h9q1-0p82></p>.
36. Steiger, N. J., Steig, E. J., Dee, S. G., Roe, G. H. & Hakim, G. J. Climate reconstruction using data assimilation of water isotope ratios from ice cores. *Journal of Geophysical Research: Atmospheres* **122**, 1545–1568 (2017).
37. Hou, J., D'Andrea, W. J. & Huang, Y. Can sedimentary leaf waxes record *D/H* ratios of continental precipitation? Field, model, and experimental assessments. *Geochimica et Cosmochimica Acta* **72**, 3503–3517 (2008).
38. Rull, V. *et al.* Late Holocene vegetation dynamics and deforestation in Rano Aroi: Implications for Easter Island's ecological and cultural history. *Quaternary Science Reviews* **126**, 219–226 (2015).
39. Butler, K. R. & Flenley, J. R. The Rano Kau 2 Pollen Diagram: Palaeoecology Revealed. (2010).
40. McFarlin, J. M., Axford, Y., Masterson, A. L. & Osburn, M. R. Calibration of modern sedimentary  $\delta^2\text{H}$  plant wax-water relationships in Greenland lakes. *Quaternary Science Reviews* **225**, 105978 (2019).

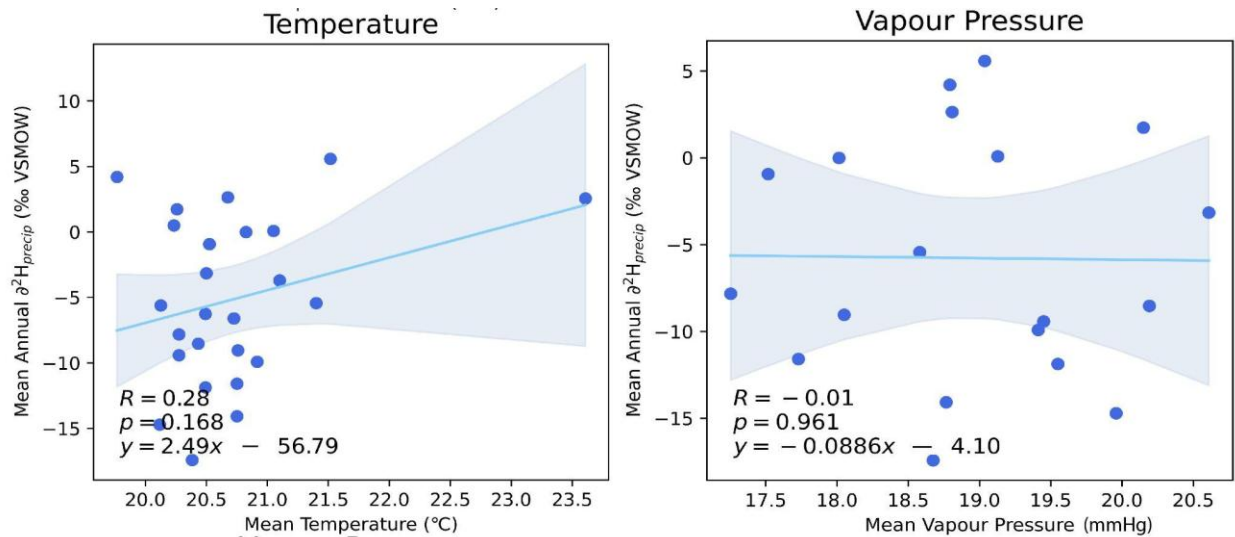
41. Jackson-Stepowski, S. & Gabon-Bautista, A. The Easter island sheep farm cultural landscape. *Historic Environment* **31**, 28–39 (2021).
42. Porteous, J. D. Easter Island: The Scottish Connection. *Geographical Review* **68**, 145–156 (1978).
43. Giraldo, M. Chill waters, arid land: climate change arrives on Easter Island. *Reuters* (2019).
44. Cañellas-Boltà, N. *et al.* Vegetation changes and human settlement of Easter Island during the last millennia: a multiproxy study of the Lake Raraku sediments. *Quaternary Science Reviews* **72**, 36–48 (2013).
45. Roman, M. *et al.* A multi-decadal geochemical record from Rano Aroi (Easter Island/Rapa Nui): Implications for the environment, climate and humans during the last two millennia. *Quaternary Science Reviews* **268**, 107115 (2021).
46. Thompson, L. G., Mosley-Thompson, E., Dansgaard, W. & Grootes, P. M. The Little Ice Age as Recorded in the Stratigraphy of the Tropical Quelccaya Ice Cap. *Science* **234**, 361–364 (1986).
47. Reuter, J. *et al.* A new perspective on the hydroclimate variability in northern South America during the Little Ice Age. *Geophysical Research Letters* **36**, (2009).
48. Bernal, J. P. *et al.* High-resolution Holocene South American monsoon history recorded by a speleothem from Botuverá Cave, Brazil. *Earth and Planetary Science Letters* **450**, 186–196 (2016).
49. Rodwell, M. J. & Hoskins, B. J. Subtropical Anticyclones and Summer Monsoons. *Journal of Climate* **14**, 3192–3211 (2001).
50. Rull, V. Drought, freshwater availability and cultural resilience on Easter Island (SE Pacific) during the Little Ice Age. *The Holocene* **30**, 774–780 (2020).
51. DiNapoli, R. J., Lipo, C. P., de Smet, T. S. & Hunt, T. L. Thermal Imaging Shows Submarine Groundwater Discharge Plumes Associated with Ancient Settlements on Rapa Nui (Easter Island, Chile). *Remote Sensing* **13**, 2531 (2021).
52. DiNapoli, R. J. *et al.* Rapa Nui (Easter Island) monument (ahu) locations explained by freshwater sources. *PLOS ONE* **14**, e0210409 (2019).
53. Morrison, A. E. An archaeological analysis of Rapa Nui settlement structure: A multi-scalar approach. (University of Hawai'i at Manoa, United States -- Hawaii) (2012).
54. Métraux A. Easter Island; a Stone-Age Civilization of the Pacific. New York: Oxford University Press; 1957

55. Davis, D. S., DiNapoli, R. J., Pakarati, G., Hunt, T. L. & Lipo, C. P. Island-wide characterization of agricultural production challenges the demographic collapse hypothesis for Rapa Nui (Easter Island). *Science Advances* **10**, eado1459 (2024).
56. Wozniak JA. Prehistoric Horticultural Practices on Easter Island: Lithic Mulched Gardens and Field Systems. *Rapa Nui J.* 1999;13: 95–99.
57. Skrzypek, G., Dogramaci, S., Page, G. F. M., Rouillard, A. & Grierson, P. F. Unique stable isotope signatures of large cyclonic events as a tracer of soil moisture dynamics in the semiarid subtropics. *Journal of Hydrology* **578**, 124124 (2019).
58. Margalef, O. *et al.* A 70,000 year multiproxy record of climatic and environmental change from Rano Aroi peatland (Easter Island). *Global and Planetary Change* **108**, 72–84 (2013).
59. Polissar, P. J. & D'Andrea, W. J. Uncertainty in paleohydrologic reconstructions from molecular  $\delta D$  values. *Geochimica et Cosmochimica Acta* **129**, 146–156 (2014).
60. Vandergoes, M. J. & Prior, C. A. AMS Dating of Pollen Concentrates—A Methodological Study of Late Quaternary Sediments from South Westland, New Zealand. *Radiocarbon* **45**, 479–491 (2003).
61. Blaauw, M. & Christen, J. A. Flexible paleoclimate age-depth models using an autoregressive gamma process. *Bayesian Analysis* **6**, 457–474 (2011).
62. Horrocks, M. *et al.* A plant microfossil record of Late Quaternary environments and human activity from Rano Aroi and surroundings, Easter Island. *Journal of Paleolimnology* **54**, 279–303 (2015).
63. Xie, P. & Arkin, P. A. Global Precipitation: A 17-Year Monthly Analysis Based on Gauge Observations, Satellite Estimates, and Numerical Model Outputs. *Bulletin of the American Meteorological Society* **78**, 2539–2558 (1997).
64. Reimer, R.W. & Reimer, P.J. 2025CALIBomb [WWW program] at <http://calib.org> accessed 2025-02-10

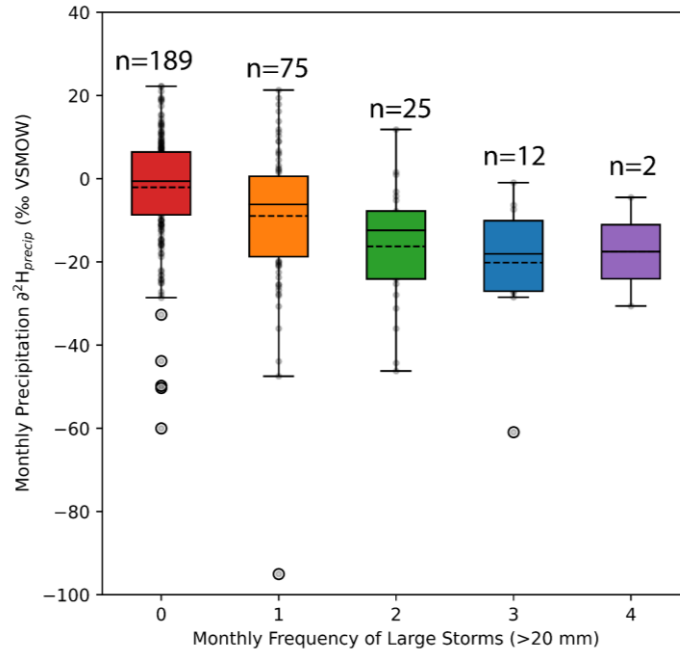
## APPENDIX



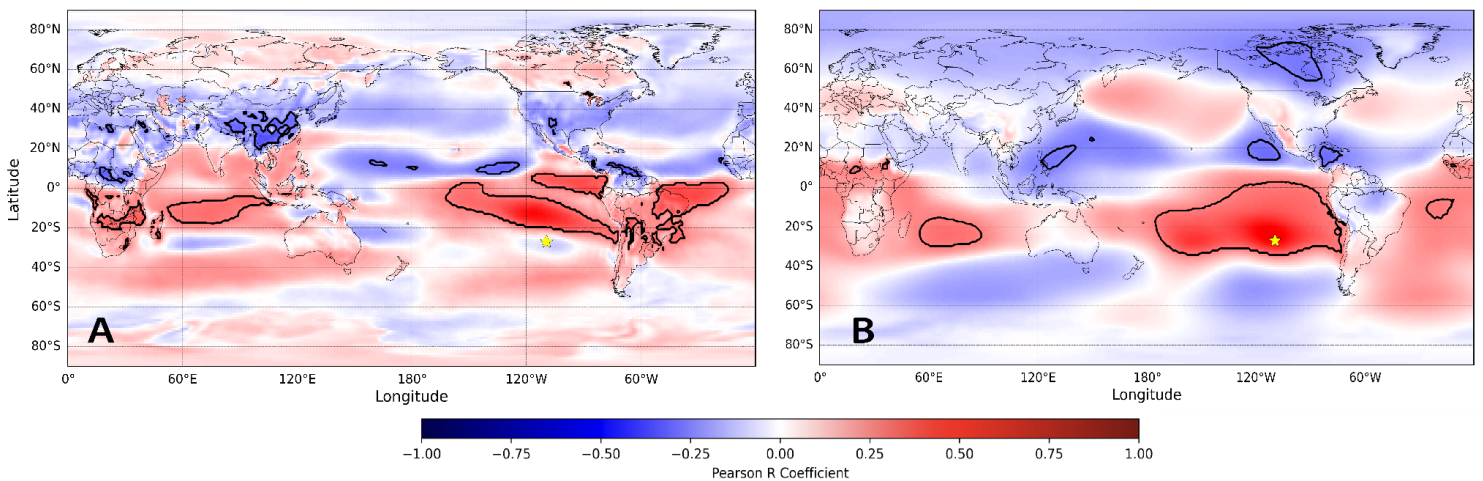
**Appendix Figure 1:** DJF average daily rainfall (1991-2020) produced from the Climate Prediction Center Merged Analysis of Precipitation<sup>63</sup>. The Intertropical Convergence Zone (ITCZ), South Pacific Convergence Zone (SPCZ), and South Pacific Anticyclone (SPA) are labeled. Rapa Nui is starred.



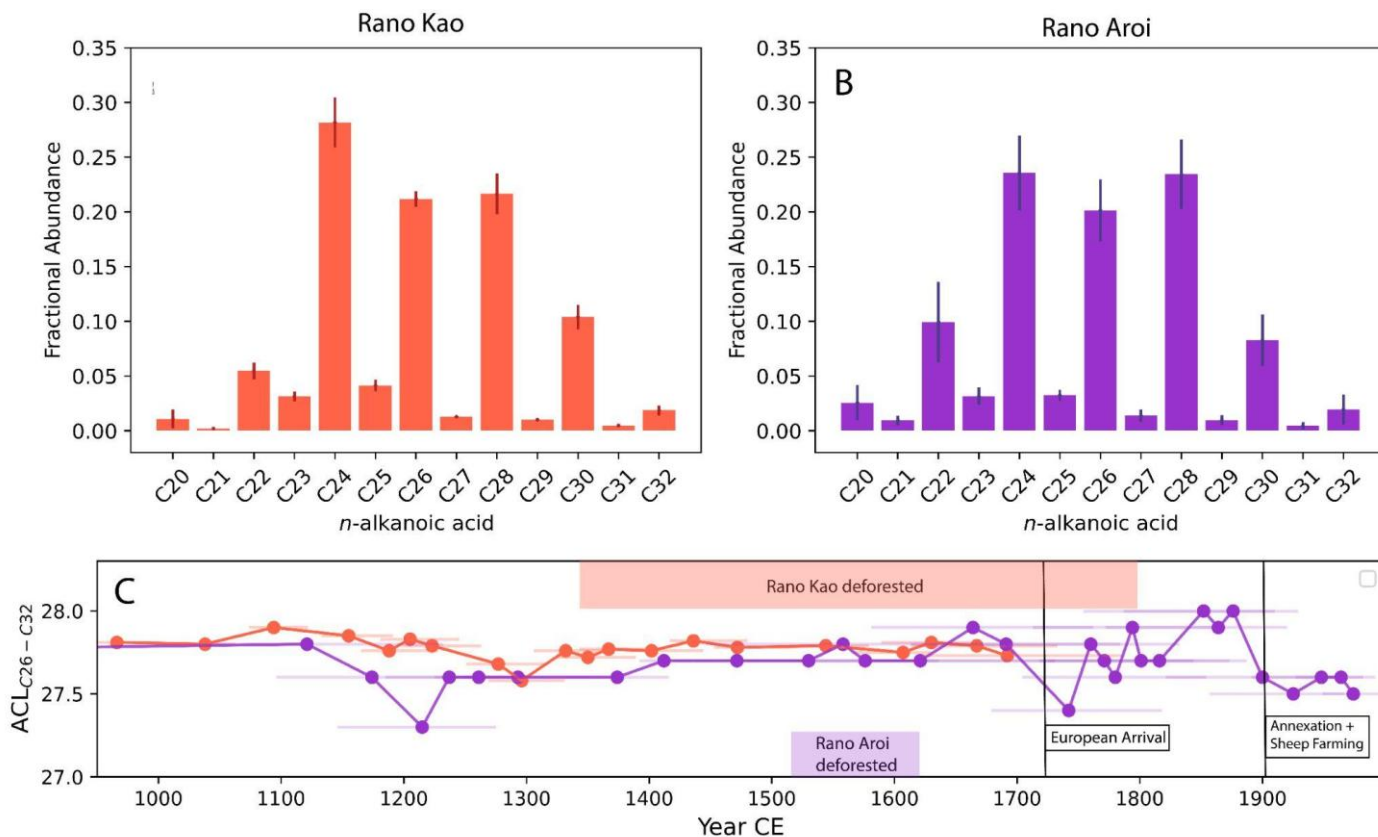
**Appendix Figure 2:** Mean annual precipitation-weighted  $\delta^2\text{H}_{\text{precip}}$  from the Global Network of Isotopes in Precipitation (GNIP) database, compared with annual mean temperature [A] and [B] vapor pressure over Rapa Nui. Neither linear regression shows significant correlation ( $p \gg 0.05$ )



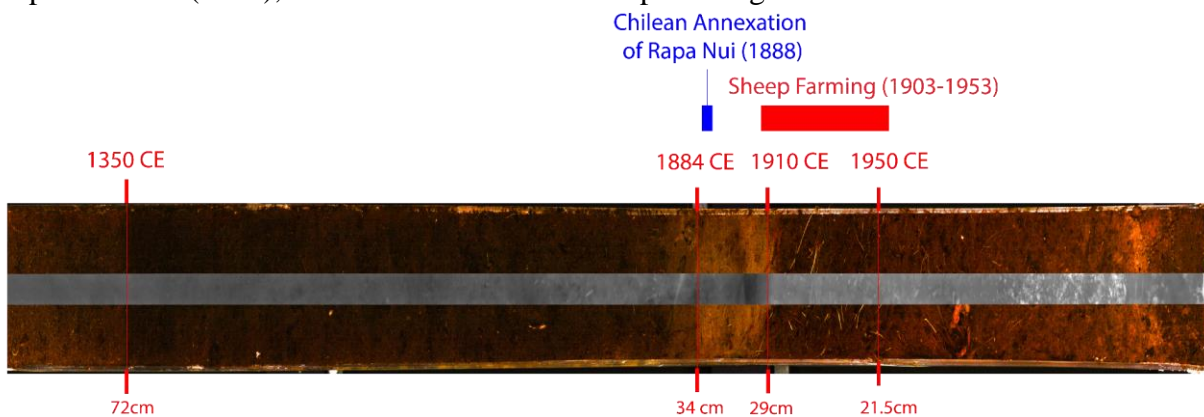
**Appendix Figure 3:** Monthly frequency of large storms, defined by Steiger et al. (2022) as storms producing >20 mm of rainfall, compared with monthly  $\delta^2\text{H}_{\text{precip}}$  over Rapa Nui from the Global Network of Isotopes in Precipitation. Solid black lines indicate median values, while dashed lines indicate means.



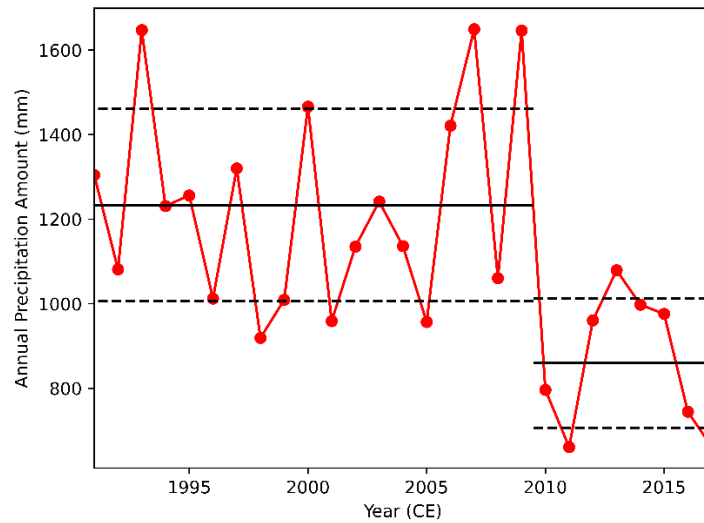
**Appendix Figure 4:** Pearson regression coefficients for monthly ECHAM5-wiso simulated  $\delta^2\text{H}_{\text{precip}}$  values over Rapa Nui (1871-2011) and the surrounding region ( $7^\circ \times 7^\circ$  grid centered on Rapa Nui grid cell) compared against the simulated [A] global 10m wind speeds and [B] sea level pressures. Black contours represent a significance level of  $p < 1e-24$ . The location of Rapa Nui is starred.



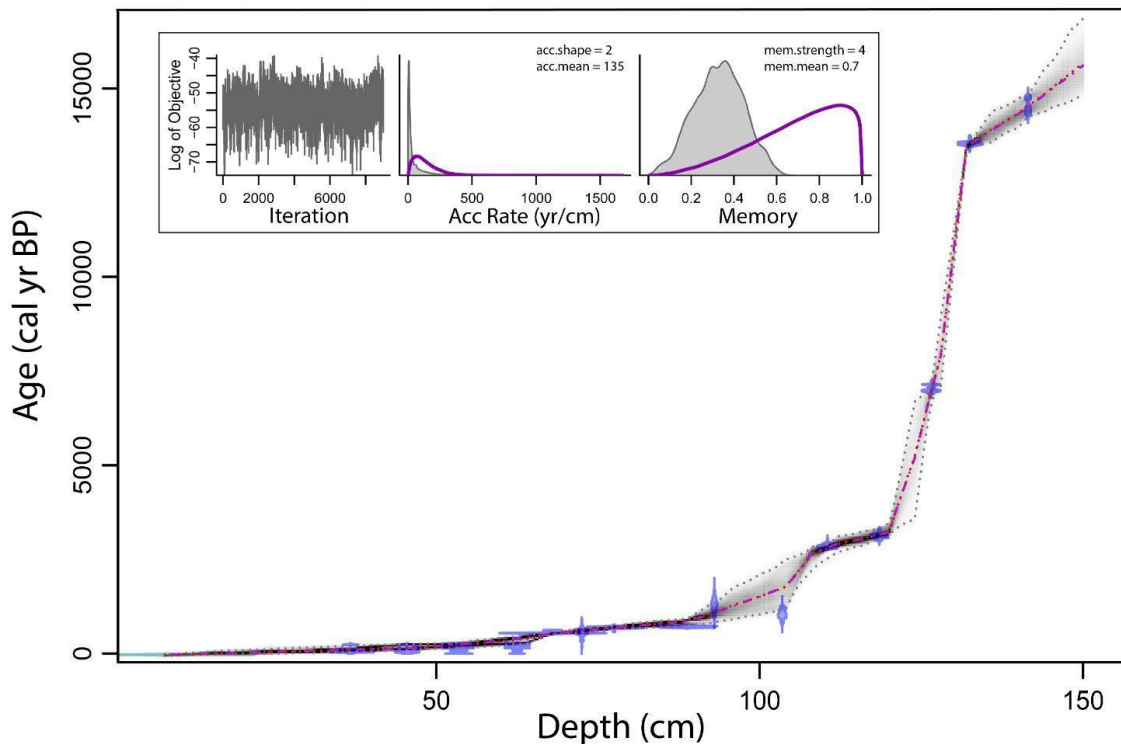
**Appendix Figure 5:** Average sedimentary *n*-alkanoic acid distributions for [A] Rano Kao and [B] Rano Aroi sediments. Error bars represent 95% confidence intervals. [C] ACL<sub>C26-C32</sub> for Rano Aroi and Rano Kao through time. The approximate timing of deforestation at each site<sup>38,39</sup>, European arrival (1722), and onset of extensive sheep farming<sup>42</sup> are indicated.



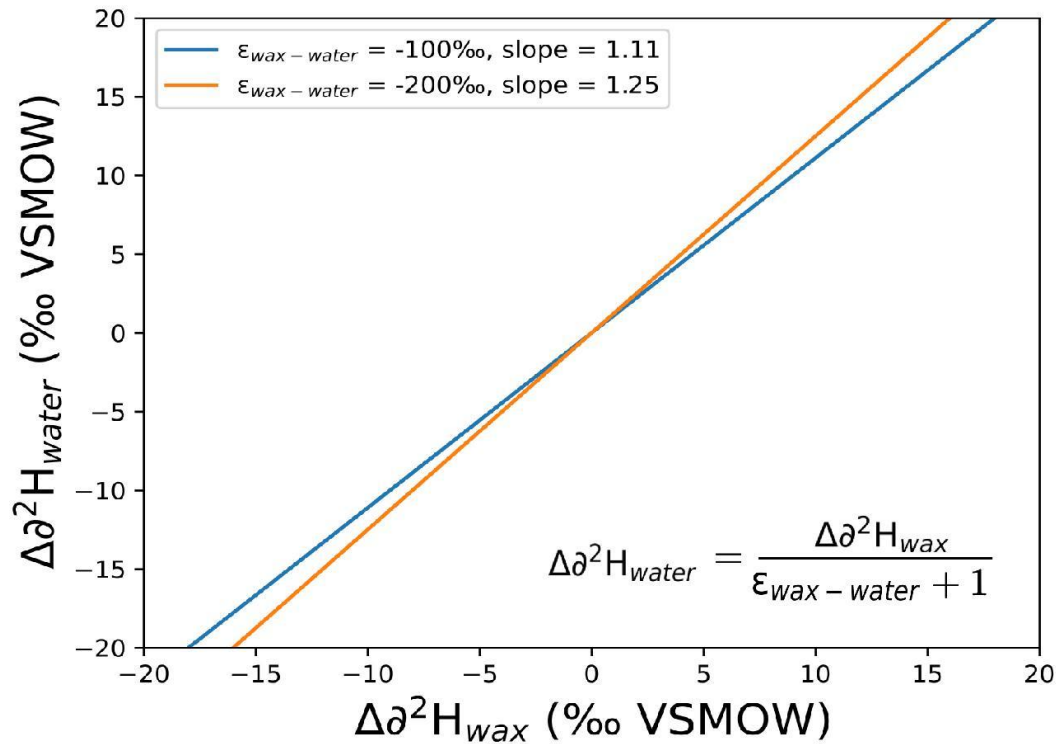
**Appendix Figure 6:** Rano Aroi core RAP-01-18 Drive 1. Significant changes in sedimentology are highlighted, specifically those that align with Chilean annexation of Rapa Nui (1888 CE) and the conversion of the island to a sheep farm under the Williamson-Balfour Company (1903-1953 CE)<sup>41,42</sup>. Sediments become significantly more fibrous and denser during this time period, and accumulation rates increase rapidly.



**Appendix Figure 7:** Annual precipitation amount over Rapa Nui from 1990-2017, calculated from monthly data provided by the Global Network for Isotopes in Precipitation (GNIP). Solid black bars represent the mean values for the intervals 1990-2009 and 2010-2017. Dashed lines represent one standard deviation.



**Appendix Figure 8.** Age model for core RAP-0118-D1 from Rano Aroi wetland, developed using the software Bacon<sup>61</sup>. Model parameters, displayed in red text, are based on previous studies of Rano Aroi<sup>58,62</sup>. Gray contours represent 95% confidence intervals. The central red line represents a mean age estimate.



**Appendix Figure 9:** Relationship between  $\Delta\delta^2H_{wax}$  and  $\Delta\delta^2H_{source\ water}$  as a function of apparent fractionation ( $\epsilon_{wax-water}$ ). Equation adapted from Polissar & D'Andrea (2014). Slopes show a small range as a function of extreme changes in  $\epsilon_{wax-water}$  (100‰).

**Appendix Table 1:** AMS  $^{14}C$  dates for terrestrial macrofossils and pollen extracts from the Rano Aroi wetland sediment core. Macrofossil material includes terrestrial organic plant matter  $>125\mu m$  (i.e. seeds, wood, leaf-fragments, plant epidermis). All macrofossil samples contain a combination of these materials, with the exception of Wood 1-RAP0118\_D1, which was a single piece of wood.

Laboratory ID	$^{14}C$ age (BP)	±	D14C (‰)	±	Core Depth (cm)
Macro 12-RAP0118_D1	Modern	5	284.9	2.3	8
Wood 1-RAP0118_D1	95	20	-11.9	2.0	36.75
Macro 15-RAP0118_D1	130	15	-16.0	1.8	45.5
Macro 43-RAP0118_D1	185	15	-22.8	1.7	53.5

Macro 44- RAP0118_D1	200	20	-24.3	2.0	62.5
Macro 100- RAP0118_D1	585	15	-70.5	1.5	68
Macro 46- RAP0118_D1	600	110	-72.3	12.1	72.5
Macro 06- RAP0118_D1	805	20	-95.3	1.9	77.5
Macro 103- RAP0118_D1	855	15	-101.1	1.5	88.75
Macro 40- RAP0118_D1	1440	140	-164.1	13.8	93
Macro 45- RAP0118_D1	1170	100	-135.1	9.9	103.5
Pollen 16- RAP0118_D1	2790	25	-293.5	2.0	110.5
Macro 102- RAP0118_D1	3000	15	-311.5	1.1	118.5
Macro 101- RAP0118_D1	6155	15	-535.2	0.9	126.5
Macro 41- RAP0118_D1	11710	30	-767.3	0.8	132.5
Macro 11- RAP0118_D1	12430	25	-787.1	0.6	141.5